

# Optical Engineering

OpticalEngineering.SPIEDigitalLibrary.org

## Terahertz confocal microscopy with an injection-seeded terahertz parametric generator

Weipeng Kong  
Zeyu Li  
Guangbin Li  
Qiang Yan  
Mingrui Zou  
Xun Zhou  
Yu Qin

Weipeng Kong, Zeyu Li, Guangbin Li, Qiang Yan, Mingrui Zou, Xun Zhou, Yu Qin, "Terahertz confocal microscopy with an injection-seeded terahertz parametric generator," *Opt. Eng.* **58**(6), 060503 (2019), doi: 10.1117/1.OE.58.6.060503.

**SPIE.**

# Terahertz confocal microscopy with an injection-seeded terahertz parametric generator

Weipeng Kong, Zeyu Li, Guangbin Li, Qiang Yan,  
Mingrui Zou, Xun Zhou, and Yu Qin\*

China Academy of Engineering Physics, Research Center  
of Laser Fusion, Mianyang, China

**Abstract.** We report on the implementation of a confocal microscopy system based on an injection-seeded terahertz parametric generator working at 1.76 THz. The system has a fairly reliable long-term stable operation with pulse energy fluctuations <5%. We experimentally demonstrate a subwavelength lateral resolution of 158  $\mu\text{m}$ , corresponding to 0.93 $\lambda$ . We also demonstrate the capability of resolving overlapping objects at the different longitudinal surfaces by imaging a designed sample. This is the first detailed demonstration of confocal microscopy based on a THz parametric source, which is helpful for the practical application of THz imaging technology. © The Authors. Published by SPIE under a Creative Commons Attribution 4.0 Unported License. Distribution or reproduction of this work in whole or in part requires full attribution of the original publication, including its DOI. [DOI: [10.1117/1.OE.58.060503](https://doi.org/10.1117/1.OE.58.060503)]

Keywords: terahertz imaging; infrared and far-infrared lasers; confocal microscopy.

Paper 190444L received Apr. 3, 2019; accepted for publication May 29, 2019; published online Jun. 14, 2019.

## 1 Introduction

Terahertz (THz) confocal microscopy is very promising for THz nondestructive testing and industry quality inspection.<sup>1–5</sup> As THz waves can penetrate nonpolar and nonmetallic materials, confocal technology can enhance resolution and achieve optical sectioning.<sup>6,7</sup> Many efforts have been made in the field of THz confocal microscopy. Salhi et al.<sup>8</sup> first introduced a transmission confocal microscope by utilizing an optically pumped THz gas laser working at 2.52 THz. Zinov'ev et al.<sup>9</sup> reported on a configuration of confocal spatial filtering using a THz photoconductive antenna. Cumis et al.<sup>10</sup> reported on the implementation of a confocal microscopy system based on a 2.9-THz quantum cascade laser operating at the temperature of 29 K. Li et al.<sup>11</sup> presented a dual-axis reflection confocal microscope system working at 2.52 THz supported by an optically pumped THz gas laser.

The injection-seeded terahertz parametric generator (is-TPG) has been dramatically improved both in output power and sensitive detection technology since 2012.<sup>12</sup> The development of is-TPG allows building THz confocal microscopy systems that are not only compact but also operating at room temperature. In addition, the tunability of is-TPG is one of

the best merits compared with other monochromatic THz sources mentioned above.

In this work, we demonstrate a THz confocal microscopy based on an is-TPG working at a frequency of 1.76 THz. The system has considerable reliability for long-term stable operation. The lateral resolution of subwavelength is achieved. We also show the experiment for axial sections imaging.

## 2 Experimental Setup

The schematic diagram of the experimental setup for the THz confocal microscopy is shown in Fig. 1. The employed is-TPG was working at 1.76 THz, corresponding to a wavelength of 170  $\mu\text{m}$ . The output pulse energy was about 1.1  $\mu\text{J}$  with the repetition rate of 100 Hz. The THz beam is collimated by an  $f = 50$  mm Tsurupica cylinder lens (L1) and focused by an  $f = 100$  mm Tsurupica lens into the first pinhole (PH1). PH1 has a diameter of  $\sim 1$  mm. Parabolic mirrors (PM1 and PM2) are used to deliver and focus the THz beam to the sample; the other two parabolic mirrors (PM3 and PM4) are applied to collect and focus the THz beam into the detector (Golay Cell, Tydex, Inc.: GC-1D). PH2 (0.5-mm large in diameter) is the second confocal pinhole located in front of the detector. The sample is mounted on an x-y-z scanner. The numerical aperture (NA) of PM1, PM2, PM3, and PM4 are 0.124, 0.447, 0.447, and 0.243, respectively. As the average power of is-TPG is relatively low, the choices of pinholes are mainly based on the sensitivity of the detector. For PM2 and PM3, we chose the mirrors with the largest NA in our lab, while keeping enough space for sample scanning.

We fixed a pinhole with 0.5-mm diameter in front of the detector and put the detector at the position where the beam pattern was to be measured. By scanning the detector in  $x$  and  $y$  axes, and recording the energy, the beam patterns were obtained. The original output beam pattern directly from is-TPG is shown in Fig. 2(a). The measurement was carried out at the position of L1 while the lenses were not located. The divergence of the beam along the  $y$  axis is much larger than that along the  $x$  axis. The beam pattern at the focal plane between PM2 and PM3 is shown in Fig. 2(b). A round beam shape in Fig. 2(b) benefits from the cylinder lens and PH1.

The stability of the system was measured for long-term operation with the is-TPG output energy of 1.1  $\mu\text{J}/\text{pulse}$ . THz waves were chopped to the frequency of 5 Hz, and then detected by the Golay Cell with a lock-in amplifier (lock-in frequency: 5 Hz). Figure 3 shows the fluctuation of THz-wave output energy within 12 h. Each dot indicates the sum of the energy of 10 pulses. Based on the root mean square error equation  $\Delta\bar{E} = \{\sum_{i=1}^n (E_i - \bar{E})^2\}/n\}^{1/2}$ , where  $E_i$  is the measured energy in the  $i$ 'th measurement,  $\bar{E} = \sum_{i=1}^n E_i/n$ ,  $\Delta\bar{E}$  was calculated to be 1.5%, and then the single-pulse energy fluctuation was calculated to be  $\sqrt{10}\Delta\bar{E} = 4.88\%$ .

We employed the knife-edge method to measure the scanning spot size around the focal plane.<sup>13</sup> We recorded the intensity profiles of  $x$  and  $y$  axes by sequentially blocking the beam with a knife blade. Then we fitted the intensity profiles to the Gaussian function to get the beam widths. The result is shown in Fig. 4, which is the full-width at half-maximum (FWHM) as a function of  $z$ . The minimum values of FWHM on  $x$  axis and  $y$  axis are 238 and 255  $\mu\text{m}$ , respectively. Microscope resolution is directly related to

\*Address all correspondence to Yu Qin, E-mail: [qiny1984@163.com](mailto:qiny1984@163.com)

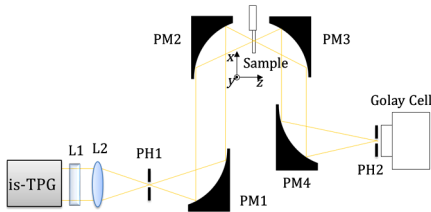


**Fig. 1** Scheme of the confocal THz microscope.

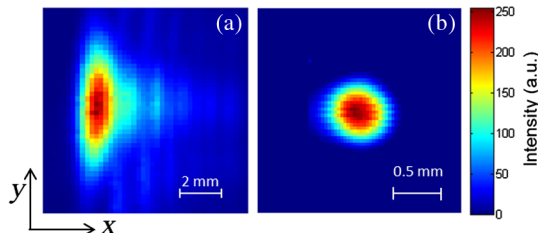


**Fig. 2** (a) The original output beam pattern directly from is-TPG at the position of L1 and (b) the focus beam pattern around the focal plane between PM2 and PM3. Both beam patterns are normalized to their maxima.

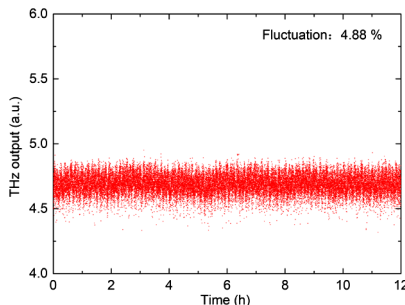


**Fig. 3** Long-term (12 h) stability of the is-TPG output.

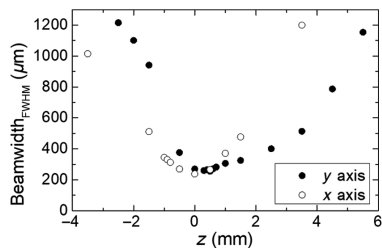


**Fig. 4** Beam FWHM along the  $z$  axis around the focal plane, obtained with the knife-edge method.

the FWHM of point spread function. Measurements of resolution utilizing the FWHM values are somewhat smaller than those calculated employing the Rayleigh criterion. The estimated lateral resolution is  $152 \mu\text{m}$  and the estimated axial resolution is  $596 \mu\text{m}$  using:  $r_{\text{lateral}} = 0.4\lambda/\text{NA}$  and  $r_{\text{axial}} = 0.7\lambda/\text{NA}^2$ ,<sup>8,14</sup> where NA is set to 0.447.

### 3 Experimental Results

The lateral resolution of the microscope based on the is-TPG was tested using a 1951 USAF resolution test plate (Edmund Optics Inc.). By scanning the test plate in two dimensions

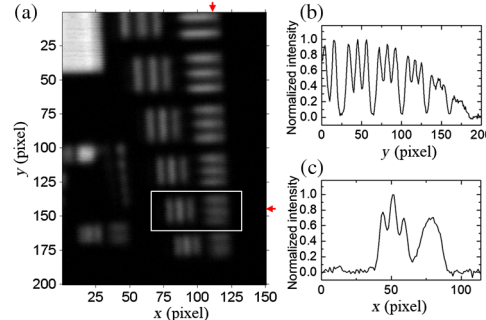


**Fig. 5** (a) Measured THz image of a 1951 USAF resolution testing plate and the normalized 1-D intensity distributions along (b) the 110th column and (c) 145th row. The solid box in (a) shows the position of line pairs 5, whereas the arrows in (a) show the locations of the 110th column and 145th row.

at the focal plane, the THz image is obtained as shown in Fig. 5(a). The area of the image has a dimension of  $20 \times 15 \text{ mm}^2$  ( $200 \times 150$  pixels), the resolution of  $x$  and  $y$  axes is better than  $3.17 \text{ lp/mm}$  [line pairs indicated by the rectangle box in Fig. 5(a)], which corresponds to  $158 \mu\text{m}$ . Figures 5(b) and 5(c) show the 1-D intensity distributions along the 110'th column and 145'th row, respectively [indicated by the arrows in Fig. 5(a)]. Both curves in Figs. 5(b) and 5(c) are normalized to  $[0, 1]$ . According to the Rayleigh criterion, two lines can be resolved while the contrast  $C = (I_{\max} - I_{\min})/I_{\max}$  is larger than 0.265,<sup>15</sup> where  $I$  is the intensity. Calculated by the results shown in Figs. 5(b) and 5(c), the contrasts in  $x$  and  $y$  direction are 0.523 and 0.343, respectively, which are larger than the critical value of 0.265.

Furthermore, we designed an experiment to show the capability of axial sectioning. Two hairs are stuck to the front and back surfaces of a 2-mm-thick TPX plate using Scotch tapes as the sample. The sample is moved along the  $z$  axis between PM2 and PM3. Figure 6(a) shows the schematics of the experimental arrangement. Figures 6(b) and 6(c) were captured when the front and back surfaces of the TPX plate were just at the focal plane. The scanning dimension was  $12 \times 12 \text{ mm}^2$  ( $120 \times 120$  pixels), and the scanning time was 4 h for each picture. The position of the hair and tapes on both sides can be identified by the intensity level and imaging clarity. We can make judgments that the vertical hair and lateral tapes are located on the front surface, while the horizontal hair and longitudinal tapes are located on the back

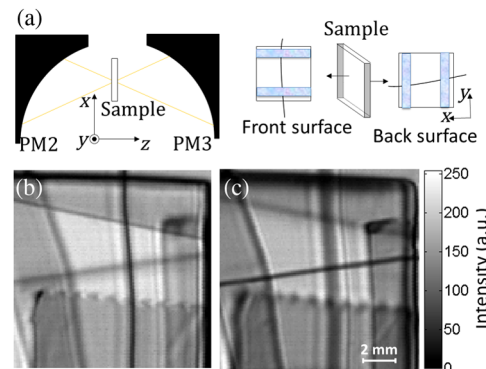


**Fig. 6** (a) Schematic diagrams of the experimental setup and measured THz image of (b) front and (c) back surfaces of the sample.

surface. The uncleanness of the elements in Fig. 6(c) is due to the contrast reduction caused by the loss of THz energy due to reflection and scattering.

#### 4 Conclusions and Outlook

In this letter, we present the THz confocal microscopy system based on an is-TPG. The is-TPG provides stable THz output during the whole scanning process with the single-pulse energy fluctuation less than 5%. The subwavelength lateral resolution of  $158\text{ }\mu\text{m}$  is achieved at 1.76 THz. In addition, the system is also capable to resolve objects located at the front and back surfaces of the sample in the designed experiment. Resolution and contrast can be further improved by increasing the NA and reducing the size of the pinholes in the current system.

It is worth mentioning that a considerable amount of the energy was lost due to the numerous optical components on the beam path. The efficiency of the microscope is  $<0.1\%$ . With the low-average power of is-TPG, more sensitive detection methods like up-conversion detection is necessary for future work that allows the system to achieve a dynamic range up to 70 dB.<sup>12</sup> We also notice that the repetition rate of the is-TPG system has reached up to 100 kHz, which means the acquisition time can be shortened to 1/150 by modification of the pump method.<sup>16</sup> Furthermore, pulse energy fluctuations can be calibrated using the pump or idler light in the parametric process to achieve better stability.

It is foreseeable that in the future, with the improvements of the THz parametric source and sensitive detection method, the image quality of the THz confocal microscopy based on is-TPG can be greatly improved, and such a system can be very practical in the 1- to 2.6-THz band.

#### Acknowledgments

This work was supported by the National Natural Science Foundation of China (No. 11804320).

#### References

1. J. B. Jackson et al., "Terahertz imaging for non-destructive evaluation of mural paintings," *Opt. Commun.* **281**(4), 527–532 (2008).
2. S. Wietzker et al., "Terahertz imaging: a new non-destructive technique for the quality control of plastic weld joints," *J. Eur. Opt. Soc. Rapid Publ.* **2**, 07013 (2007).
3. F. Rutz et al., "Terahertz quality control of polymeric products," *Int. J. Infrared Millimeter Waves* **27**(4), 547–556 (2006).
4. N. Karpowicz et al., "Non-destructive sub-THz CW imaging," *Proc. SPIE* **5727**, 132–142 (2005).
5. W. E. Baughman et al., "Comparative reconstructions of THz spectroscopic imaging for non-destructive testing and biomedical imaging," *Proc. SPIE* **8363**, 21 (2012).
6. M. Tonouchi, "Cutting-edge terahertz technology," *Nat. Photonics* **1**(2), 97–105 (2007).
7. M. Minsky, "Memoir on inventing the confocal scanning microscope," *Scanning* **10**(4), 128–138 (1988).
8. M. Salhi, P. Ioachim, and K. Martin, "Confocal THz laser microscope," *Int. J. Infrared Millimeter Waves* **31**(3), 358–366 (2009).
9. N. N. Zinov'ev and A. V. Andrianov, "Confocal terahertz imaging," *Appl. Phys. Lett.* **95**(1), 011114 (2009).
10. U. S. D. Cumis et al., "Terahertz confocal microscopy with a quantum cascade laser source," *Opt. Express* **20**(20), 21924–21931 (2012).
11. Q. Li et al., "2.52 terahertz dual-axis reflection confocal scanning microscope," *J. Opt. Soc. Am. A* **33**(4), 637–641 (2016).
12. H. Minamide et al., "Kilowatt-peak terahertz-wave generation and sub-femtojoule terahertz-wave pulse detection based on nonlinear optical wavelength-conversion at room temperature," *J. Infrared Millimeter Terahertz Waves* **35**(1), 25–37 (2014).
13. Y. Qin et al., "Characterization of non-Gaussian mid-infrared free-electron laser beams by the knife-edge method," *Infrared Phys. Technol.* **66**, 146–151 (2014).
14. N. S. Claxton, T. Fellers, and M. Davidson, "Laser scanning confocal microscopy," <http://www.aptechnologies.co.uk/images/Data/Vertilon/PP6207.pdf> (2006).
15. G. S. Kino and R. C. Timothy, *Confocal Scanning Optical Microscopy and Related Imaging Systems*, Academic Press, San Diego (1996).
16. Y. Moriguchi et al., "High-average and high-peak output-power terahertz-wave generation by optical parametric down-conversion in MgO:LiNbO<sub>3</sub>," *Appl. Phys. Lett.* **113**(12), 121103 (2018).